Surface plasmons and strong light-matter coupling in metallic nanoshells

Filippo Alpeggiani, Stefania D'Agostino, and Lucio Claudio Andreani
Dipartimento di Fisica, Università degli Studi di Pavia, Via Bassi 6, 27100 Pavia, Italy
(Received 17 May 2012; published 16 July 2012)

A theory of the interaction between a radiating dipole and the plasmonic excitations of a spherical metallic nanoshell in the quasistatic approximation is formulated. After a derivation of surface plasmon frequencies and a comparison with the corresponding modes of metal spheres and cavities, we introduce an expression for the effective volume for any position of the dipole inside or outside the nanoshell, describing the local electromagnetic field enhancement in analogy to other cavity-QED systems. The modification of the dipole decay rate is calculated as a function of frequency for various geometrical parameters, and it reflects the spectrum of spherelike and cavity-like surface plasmon excitations. We then give a formulation of emission spectra, suitable for describing light-matter interaction beyond perturbation theory, and study the conditions for the strong coupling regime to occur. By suitably tuning the geometrical parameters of the nanoshell and by choosing the order of surface plasmon modes to minimize the effective volume, a vacuum Rabi splitting can occur in emission spectra for dipole oscillator strengths as small as a few units, which can be easily achieved with organic molecules or quantum dots. The most favorable situation for strong coupling is when the dipole is located inside the nanoshell. Surprisingly, this dipole couples with spherelike modes more strongly than with cavity-like ones, if the shell is thin enough. As a conclusion, metallic nanoshells turn out to be a suitable platform in order to investigate the strong-coupling regime of light-matter interaction by exploiting surface plasmon resonances.

DOI: 10.1103/PhysRevB.86.035421 PACS number(s): 73.20.Mf, 78.20.Bh, 78.67.Bf

I. INTRODUCTION

The spontaneous decay of a system represents not only a fundamental phenomenon in the study of radiation-matter interaction, but also the starting point for a wide range of conceptual and technological developments. As already pointed out in the pioneering work by Purcell,[1] it is possible to control the emission rate by modifying the local environment. A strong boost in this direction has come from the rapidly developing field of plasmonics, i.e., metallic optics at the nanoscale. A key advantage of plasmonic nanosystems is their ability to keep the optical energy concentrated in a subwavelength range in proximity to metallic surfaces;[2] this leads to a significant enhancement of the local density of states of the electromagnetic field, producing an increase of the spontaneous decay rate sometimes comparable with high-Q optical cavities.[3]

The natural context in which to treat the spontaneous decay is quantum electrodynamics, modeling the emitter as a generic two-level system (a "dipole"). The peculiar optical properties of metals require extending the traditional methods of quantization of the electromagnetic field to dispersive and absorbing inhomogeneous media. Following the works in Refs. 4–8, this can be performed by diagonalizing the Hamiltonian of the unperturbed system, the free-space electromagnetic field, and a continuous set of (spatially distributed) harmonic oscillators, in analogy with the Hopfield model of a dielectric.[9] A family of bosonic fields of the composite system is obtained, which are related to the actual electromagnetic field through the dyadic Green function.[10] Alternative formulations are given in Refs. 11 and 12.

In the Markov approximation, the spontaneous decay rate turns out to directly depend on the imaginary part of the dyadic Green function; by expanding the latter onto an appropriate set of wave vectors, the decay rate enhancement can be calculated analytically when the dipole is in the vicinity of spatially confined nanostructures with simple geometry, notably spherical particles,[13–16] spheroids and ellipsoids,[17,18] stratified spheres,[19–21] nanowires, and nanotips.[22] This method has a well-known classical analog in an oscillating dipole interacting with its own emitted radiation[23,24] and is particularly suitable for numerical simulations.[14,25–33] The strong localization of the electromagnetic field near the surface can be understood in terms of the excitation of surface plasmons, electronic collective oscillations, originated by a surface charge coupled with the incident electromagnetic waves.[3,34,35]

Another fruitful approach to the study of spontaneous decay is to identify the surface plasmons and to describe them with the cavity quantum electrodynamics (cQED) formalism.[36,37] The identification can be developed on the analysis of conduction electron gas deformations[38–40] or within classical electrostatic theory.[41] The study can be extended to more complex nanostructures, such as nanoshells and particle dimers, within the so-called *hybridization model*.[42,43] Composite systems can also be understood in terms of artificial optical molecules[44,45] or coupled mode systems.[46] Periodic arrays of metallic nanoparticles in three dimensions have been investigated, as well.[47] Within the quasistatic approximation, which is generally valid for small enough particles, these techniques give a clear insight into the physics of surface-plasmon excitations and light-matter coupling.

When the interaction with radiation is significantly enhanced by localization effects, the dipole can reversibly exchange excitation with the plasmonic modes, entering the strong coupling regime. The most recognizable consequence is the formation of a doublet of peaks in the emitted-light spectrum around the dipole frequency (Rabi splitting). Recently, growing interest has arisen for the study of strong coupling effects in proximity to metal nanoparticles, either via a mixed boundary-element-method/cQED approach,[48] a full cQED treatment in the dipolar approximation,[49] or a Green-function

treatment.[50] The last approach has also been applied to the case of coated spheres and particle dimers.[51] Another possible platform based on graphene has been recently proposed.[52]

In this work, we treat a dipole in proximity to a spherical metallic nanoshell with the goal of relating light-matter interaction, and especially the strong coupling regime, to surface plasmon excitations. In this sense, the present approach combines cavity quantum electrodynamics and plasmonics. A spherical nanoshell represents a promising system for enhancing light-matter interaction, since it supports both spherelike and cavity-like modes whose properties can be engineered and tuned as a function of geometrical parameters. Although analytical methods based on the dyadic Green function—which is known for this system[53]—could, in principle, be applied, here we aim at a more transparent approach in order to shed light on the dependence of light-matter coupling regimes on geometrical parameters (shell radius and thickness), in view of their optimization. As we are especially interested in small nanoparticles, which are most favorable for achieving strong light-matter coupling, we adopt the quasistatic approximation.

In Sec. II, we provide a full description of the plasmonic modes of nanoshells in terms of modal frequencies, as in Ref. 54, and also in terms of effective volumes and decay widths, which are essential to investigate decay rate modifications and strong coupling effects. The definition of the effective mode volume includes in a general way the dependence on the dipole position. The decay rate of the dipole in the perturbative regime is then calculated as a sum of Lorentzian-shaped resonances, each one potentially leading to a Purcell enhancement, and is shown to agree with that obtained from the dyadic Green function formalism in the $c \to \infty$ limit. In Sec. III, we derive an expression for the spectrum of the light emitted by the dipole when the classical decay rate is expressed as a sum of Lorentzian functions: this is useful in itself, as it could be applied when the spectrum is calculated by different (e.g., fully numerical) techniques and fitted with Lorentzian resonances. Each resonance is characterized by a Rabi frequency and a linewidth: when the former dominates over the latter, the emitted spectrum shows a two-peak structure that is characteristic of the strong coupling regime. This leads to analytic formulas for the threshold oscillator strength required for strong coupling. The formalism is then applied to the case of nanoshells, where we exploit the degrees of freedom provided by the geometrical parameters and by the spectrum of spherelike and cavity-like plasmonic modes in order to achieve the strong coupling regime while minimizing the threshold oscillator strength. For properly chosen parameters, the strong coupling regime can be achieved with relatively small oscillator strengths, which easily occur in organic molecules or quantum dots. In particular, an appropriately chosen nanoshell with the dipole placed inside can provide a better environment for strong coupling phenomena than a similarly sized nanoparticle. These results show that metal nanoshells are promising systems in view of tailoring radiation-matter interaction and exploiting surface plasmon resonances in the nonperturbative regime. Section IV contains concluding remarks. The formalism for the comparison between dyadic Green function and cQED approaches is summarized in Appendix.

II. PLASMONIC MODES IN NANOSHELLS

A. Mode frequencies

In this section, we will analyze the electromagnetic eigenmodes of a metallic shell with inner radius a and outer radius A, with a dipole located either inside or outside, as shown in Figs. 1(a) and 1(b), respectively. The metal is characterized by a dielectric function ϵ, while the remaining regions are vacuum. Here, vacuum has been chosen to reduce the number of parameters entering the model, but the theory could be easily adapted to more realistic situations involving a dielectric core. We will use the quasistatic approximation, which consists of neglecting the retardation effects everywhere except in the dielectric function dependence on the frequency. As a starting point, we consider the solutions of the Laplace equation for the electrostatic potential $\nabla^2\phi = 0$. These can be individuated by the angular momentum l and the azimuthal number $m = -l, \ldots, l$, each frequency being $2l + 1$ times degenerate with respect to m. Here, we give the expression only for modes with azimuthal symmetry ($m = 0$), which are described by means of the Legendre polynomials $\mathrm{P}_l(\cos\theta)$ in the form[55]

$$\phi_l(r,\theta) = \begin{cases} \beta_1 r^{-(l+1)}\mathrm{P}_l(\cos\theta), & r > A, \\ (\alpha_2 r^l + \beta_2 r^{-(l+1)})\mathrm{P}_l(\cos\theta), & a \leqslant r \leqslant A, \\ \alpha_3 r^l \mathrm{P}_l(\cos\theta), & r < a. \end{cases} \quad (1)$$

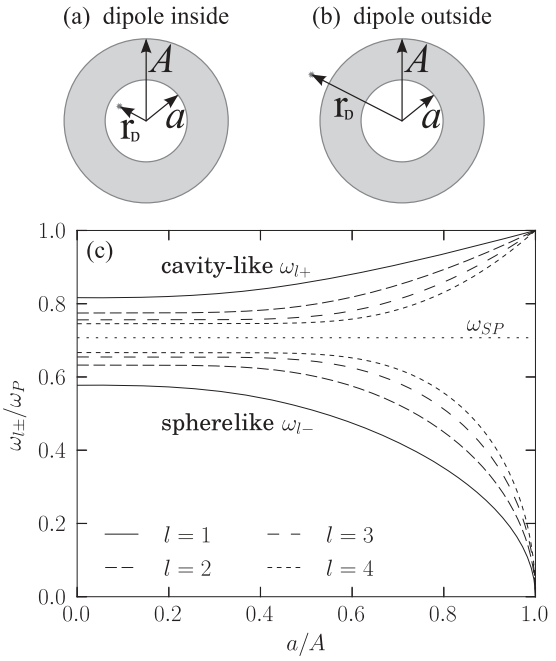

FIG. 1. Insets (a) and (b): the geometry of the two systems under consideration, constituted by a metallic shell with a dipole either inside or outside it. a and A are the inner and outer radii, respectively, whereas r_d indicates the dipole distance from the center. (c) Dispersion relation of plasmonic modes. Modal frequencies $\omega_{l\pm}$ (normalized to ω_P) are plotted for some indices l as a function of the ratio a/A. ω_SP refers to the surface plasmon frequency $\omega_\mathrm{P}/\sqrt{2}$.

The electrostatic field is obtained as $\boldsymbol{E} = -\nabla\phi$:

$$\boldsymbol{E}_l(r,\theta) = \begin{cases} \beta_1 r^{-(l+2)}\left[(l+1)\mathrm{P}_l(\cos\theta)\hat{\boldsymbol{r}} - \frac{\partial \mathrm{P}_l}{\partial\theta}(\cos\theta)\hat{\boldsymbol{\theta}}\right], & r > A, \\ [-\alpha_2 l r^{l-1} + \beta_2(l+1)r^{-(l+2)}]\mathrm{P}_l(\cos\theta)\hat{\boldsymbol{r}} - [\alpha_2 r^{l-1} + \beta_2 r^{-(l+2)}]\frac{\partial \mathrm{P}_l}{\partial\theta}(\cos\theta)\hat{\boldsymbol{\theta}}, & a \leqslant r \leqslant A, \\ -\alpha_3 r^{l-1}\left[l\mathrm{P}_l(\cos\theta)\hat{\boldsymbol{r}} + \frac{\partial \mathrm{P}_l}{\partial\theta}(\cos\theta)\hat{\boldsymbol{\theta}}\right], & r < a. \end{cases} \quad (2)$$

By imposing the continuity of the tangential and normal components of the electric field and the displacement vector, respectively, we obtain the characteristic equation

$$l(l+1)(\epsilon^2+1)\left[1-\left(\frac{a}{A}\right)^{2l+1}\right] + 2l(l+1)\epsilon\left[1+\left(\frac{a}{A}\right)^{2l+1}\right] + \epsilon = 0. \quad (3)$$

It must be solved with respect to the frequency; its solutions are the proper frequencies of the electrostatic modes. Notice that, in order to satisfy the boundary conditions, only the values $l \geqslant 1$ can be used. We suppose that the metal dielectric function follows a Drude model of the form $\epsilon(\omega) = 1 - \frac{\omega_{\mathrm{P}}^2}{\omega(\omega+i\gamma_{\mathrm{D}})}$; for instance, a choice of the parameters for silver is[56]

$$\hbar\omega_{\mathrm{P}} = 5.21 \ \mathrm{eV}, \quad \hbar\gamma_{\mathrm{D}} = 0.044 \ \mathrm{eV}. \quad (4)$$

If we neglect the imaginary (dissipative) part of the dielectric function and replace its real part in the characteristic equation (3), we obtain the set of solutions

$$\omega_{l\pm}^2 = \frac{\omega_{\mathrm{P}}^2}{2}\left[1 \pm \frac{1}{2l+1}\sqrt{1+4l(l+1)\left(\frac{a}{A}\right)^{2l+1}}\right]. \quad (5)$$

The relation between the modal frequencies and the ratio a/A is represented in Fig. 1(c) for some values of the index l. In particular, when $l \to \infty$, they tend to accumulate over the *surface plasmon frequency* $\omega_{\mathrm{SP}} = \frac{1}{\sqrt{2}}\omega_{\mathrm{P}}$. The identification of these modal frequencies has been already formulated in Ref. 54—see also Refs. 40 and 57—in the context of the so-called *hybridization model*, based on the study of the deformations of an electron gas filling the shell.

In the limit $a/A \to 0$, the characteristic equation (3) decouples in the form

$$[\epsilon l + l + 1][\epsilon(l+1) + l] = 0. \quad (6)$$

The first factor cancels out in coincidence with the well-known resonant frequencies of a solid metallic sphere,[41]

$$\omega_l^{\mathrm{sph}} = \omega_{\mathrm{P}}\sqrt{\frac{l}{2l+1}}, \quad (7)$$

whereas the second factor provides the resonant frequencies of a cavity surrounded by an infinite homogeneous metal (we will call it an "ideal cavity"),

$$\omega_l^{\mathrm{cav}} = \omega_{\mathrm{P}}\sqrt{\frac{l+1}{2l+1}}. \quad (8)$$

Notice that the modes of the cavity are always larger than the surface plasmon frequency ω_{SP}. As can be seen in Fig. 1(c), they share this property with the nanoshell modes of the form ω_{l+}, of which they represent the limit $a/A \to 0$. For this reason, we call the ω_{l+} modes of a nanoshell *cavity-like modes*. Analogously, ω_{l-} modes of a nanoshell reduce to those of a sphere in the same limit $a/A \to 0$ and are always smaller than ω_{SP}: we refer to them as *spherelike modes*. An analogous discussion has been given in Refs. 44 and 45 for the case of coupled metallic nanoparticles.

B. Interaction with the dipole and effective volumes

For a dipole in interaction with the metal nanoshell at a given position $\boldsymbol{r}_d$, we want to express the dipole decay rate from Fermi golden rule in terms of coupling with the plasmonic modes. The dipole-electromagnetic field interaction $-\boldsymbol{\mu}\cdot\boldsymbol{E}$ leads to a Purcell-like formula as a sum of Lorentzian functions centered on the frequencies $\omega_{l\pm}$, as discussed below. In addition to the modal frequencies, it is useful to express the dipole interaction in terms of an effective volume. Without lack of generality we can assume the dipole to lie along the z axis. We focus on the case of a radially oriented dipole ($\boldsymbol{\mu} \parallel \hat{\boldsymbol{r}}$), which can be shown to interact with the $m = 0$ modes only. Then, the effective volume can be defined as follows:[58]

$$V_{\mathrm{eff},l}\,|\boldsymbol{E}_l(\boldsymbol{r}_d)\cdot\hat{\boldsymbol{r}}|^2 = \frac{1}{2}\int d\boldsymbol{r}\,\frac{\partial\{\omega\,\mathrm{Re}[\epsilon(\omega)]\}}{\partial\omega}|\boldsymbol{E}_l(\boldsymbol{r})|^2, \quad (9)$$

where r_d is the dipole distance from the nanoshell center and θ_d its polar coordinate. The right-hand side of the definition is the expression for the electromagnetic energy in dispersive media.[59] Then, the effective volume corresponds to the volume of a hypothetical constant-field cavity containing the same electromagnetic energy of the plasmonic mode (in the quasistatic approximation the contribution from the magnetic field is neglected). Equation (9) has the advantage of including in a natural way the dependence on the dipole position and orientation; in particular, the smaller the effective volume, the larger is the field confinement (or localization) at the chosen location. In the case of nanoshells, it leads to results that perfectly coincide with the $c \to \infty$ limit of the analytical ones obtained from the dyadic Green function treatment, as shown in Appendix.

The *inverse* effective volume of the lth mode can be calculated in the form[60]

$$V_{\mathrm{eff},l}^{-1} = \frac{1}{4\pi}\,\frac{1-\left(\frac{a}{A}\right)^{2l+1}}{2l+1\pm\Delta}\,l(l+1) \times \begin{cases} l\,a^{-3}\,(1\pm\Delta^{-1})\left(\frac{r_d}{a}\right)^{2l-2}, & r_d < a, \\ (l+1)\,A^{-3}\,(1\mp\Delta^{-1})\left(\frac{A}{r_d}\right)^{2l+4}, & r_d > A, \end{cases} \quad (10)$$

where $\Delta = \sqrt{1+4l(l+1)\,(a/A)^{2l+1}}$. The upper sign refers to ω_{l+} modes, while the lower one to ω_{l-} modes.

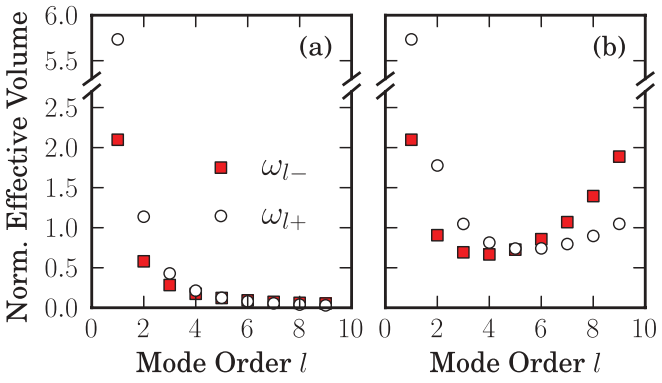

FIG. 2. (Color online) Effective volume of the plasmonic modes of a nanoshell with ratio $a/A = 0.8$ as a function of the mode order l, normalized with respect to the total volume of the nanoshell $\frac{4}{3}\pi A^3$. Circles refer to ω_{l+} modes, squares to ω_{l-} ones. In (a), the radially oriented dipole is in contact with the inner surface of the shell, whereas in (b), it is located at $r_d = 0.8a$.

The present expression applies to the case of an arbitrary position of the dipole (not necessarily at the maximum of the electric field). In particular, the nonzero distance between the dipole and the nearest metallic surface plays an important role. In Fig. 2(a), we display the effective volume of a nanoshell with ratio $a/A = 0.8$ as a function of the mode order l, supposing that the dipole is in contact with the inner surface ($r_d = a$); it corresponds to the smallest effective volume available when the dipole is inside the nanoparticle. It seems that the effective volume tends to reduce with the increasing of the order, but this behavior could lead to a deceptive interpretation. If we consider a finite distance from the surface—as in Fig. 2(b), where we have set $r_d = 0.8a$—we can observe that the effective volume diverges when $l \to \infty$, too. So, upon fixing a certain choice of the parameters of the system, there must be a well-defined mode that minimizes the effective volume. It makes perfectly sense, then, to optimize the geometry in order to tune this mode in resonance with the dipole frequency; all the following analyses and discussions try to develop this concept. Notice that the same phenomenon is observable also in nanoparticles,[61] but in that case modal frequencies are not tunable [see Eq. (7)], making the shell geometry definitely more interesting.

We now turn to the analysis of the decay rate. The decay width includes two contributions, from both radiative and nonradiative losses. In general, the quasistatic approximation does not permit to compute properly the radiative decay rate (see, for instance, Ref. 15). For the $l = 1$ mode, which presents dipolar symmetry, the radiative contribution to the modal width can be evaluated calculating the dipole moment induced by the charge density on the surface of the nanoshell;[41] higher-order modes, on the contrary, are completely radiationless in the quasistatic approximation. However, due to their small effective volumes, $l > 1$ modes are the most likely to give rise to strong-coupling effects, where the radiative or nonradiative character of the interaction makes no difference, as it will be seen in Sec. III. Since we will mainly refer to these modes, we have decided to neglect at all the radiative contribution to the modal widths. Notice that, in spite of being absent in the quasistatic approximation, radiative effects can be taken in account with more elaborate analytical models. In general, the detection of far-field radiation is not necessarily prevented by the mainly nonradiative character of the coupling. For instance, in the case of metal nanospheres discussed in Ref. 50, the radiative contribution to the decay rate, in spite of being far less significant than the nonradiative one, is enhanced with respect to the free-space decay. In other words, the overall radiative signal is increased by the presence of the nanoparticle, which acts like a "*nanoantenna*" in the sense of enhancing the radiative emission of the dipole.

In the quasistatic approximation, the nonradiative contribution to the modal width can be obtained from the dissipation rate of light in the metal as explained in Ref. 41, or solving the characteristic equation (3) with a complex frequency. In both cases, it can be shown to coincide exactly with the Drude damping constant γ_D. In order to obtain the perturbative total decay rate of a dipole with frequency ω, from the effective volume of each plasmonic mode we can calculate the corresponding *Purcell factor* $(6\pi/k^3)(Q/V_{\mathrm{eff},l}) = (3\lambda^3 Q)/(4\pi^2 V_{\mathrm{eff},l})$, weighted by a Lorentzian function of width γ_D centered on the modal frequency. Here, $k = \omega/c$ and the Q value can be estimated as the ratio $\omega_{l\pm}/\gamma_D$. By summing over all modes and taking into account the free-space decay background, we obtain the expression for the decay rate:

$$\frac{\Gamma(\omega)}{\Gamma_0(\omega)} = 1 + \frac{6\pi}{k^3}\sum_{l\geqslant 1} Q\, V_{\mathrm{eff},l}^{-1}\frac{\left(\frac{1}{2}\gamma_D\right)^2}{(\omega-\omega_{l\pm})^2 + \left(\frac{1}{2}\gamma_D\right)^2}, \qquad (11)$$

where $\Gamma_0(\omega)$ is the free-space decay rate $k^3\mu^2/3\hbar\pi\epsilon_0$. Notice that in this result, proved in the Appendix, the dependence on the geometry is embodied in the effective volume, while the linewidth of each resonance is given by the Drude damping constant γ_D. As an example of application, in Fig. 3(a) we display the decay rate of a radial dipole 2 nm away from the inner surface of a nanoshell with radii $a = 8$ nm and $A = 12$ nm as a function of the dipole frequency.

Recently, it was pointed out[62] that the use of the Purcell factor could lead to an underestimation of the correct decay rate. This happens when using a single Purcell factor originating from the whole spectrum of modes (in the assumption that it is dominated by a single term). In the present work, we keep track of the contributions of each mode separately, and the decay rate is accurately represented by the Purcell equation summed over all resonances.

C. Beyond the quasistatic approximation

The result (11) has the advantage to present the dependence on the geometrical parameters of the system in a simple workable way; however, being obtained in the quasistatic approximation, it neglects the contribution from retardation effects. As shown in the literature,[7,11,23] the exact expression of the classical decay rate of a dipole (including retardation effects) depends on the imaginary part of the dyadic Green function of the system under consideration:

$$\Gamma(\omega) = \frac{2\omega^2}{\hbar\epsilon_0 c^2}\boldsymbol{\mu}\cdot \mathrm{Im}\,\overleftrightarrow{G}(\boldsymbol{r}_d,\boldsymbol{r}_d,\omega)\cdot\boldsymbol{\mu}. \qquad (12)$$

The nanoshell is an example of a spherically layered medium, for which the dyadic Green function is known.[53] As we show

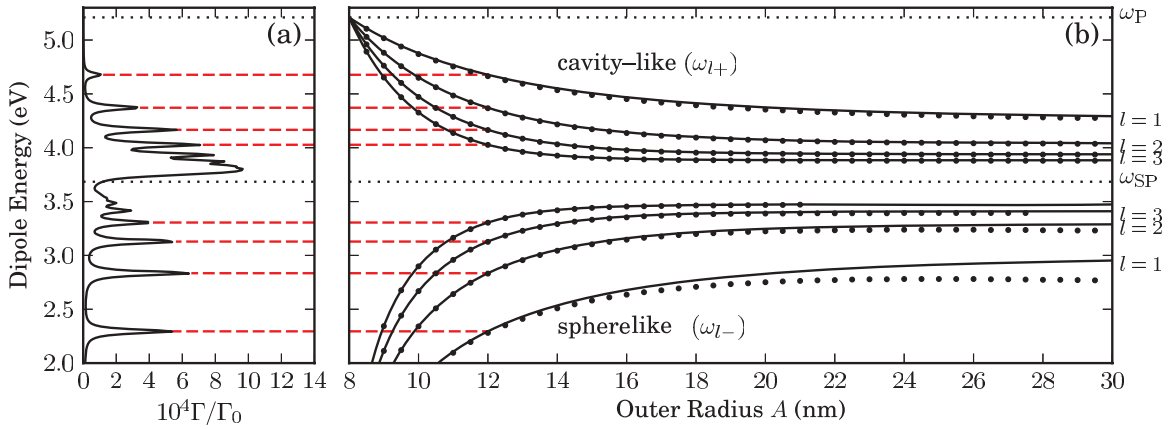

FIG. 3. (Color online) (a) Classical decay rate in the quasistatic approximation [see Eq. (11)] of a radially oriented dipole in proximity to a silver nanoshell, as a function of the dipole frequency (displayed on the y axis). The parameters of the system are $a = 8$ nm, $A = 12$ nm, and $r_d = 6$ nm. (b) Solid lines: the frequencies of the plasmonic modes of a silver nanoshell with inner radius of 8 nm vs the outer radius A (for clarity, only those up to $l = 4$ are shown). The relation with the local maxima of the classical decay rate is underlined by the dashed red lines. Dots: the local maxima of the exact classical decay rate including retardation effects, calculated with the dyadic Green function approach according to Ref. 20 for the same parameters. The dielectric function follows the Drude model [see Eq. (4)].

in Appendix, our quasistatic result can be derived also from Eq. (12) by taking the limit $c \to \infty$.

A computer script for the numerical evaluation of the exact decay rate has been developed by Moroz.[20] We used it to extract the local maxima of the decay rate (plotted as a function of the dipole frequency) for several geometries; they are shown by the dots in Fig. 3(b). When the geometrical parameters of the system are small, so that retardation effects are negligible, the agreement with the modal frequencies in Eq. (5) is very good, except for a slight redshift of the exact results with respect to the quasistatic ones, which is noticeable only for the lowest ω_{l-} modes. The redshift becomes more significant with increasing system dimensions; however, being interested in optimizing the strength of the coupling with radiation, we will consider only small systems, where localization effects are more likely to enhance the local density of states of the electromagnetic modes. Then, our quasistatic approximation is surely suitable for our aims.

D. Comparison with spheres and ideal cavities

We have previously shown that there exist two different families of nanoshell plasmonic modes, the cavity-like (ω_{l+}) and the spherelike ones (ω_{l-}). The modal frequencies of cavity-like modes revert to those of an ideal cavity [see Eq. (8)] in the limit $a/A \to 0$. Correspondingly, in the same limit, the values of the effective volume in Eq. (10) tend to the ones of an ideal cavity:

$$V_{\mathrm{cav},l} = \frac{4\pi a^{2l+1}}{l^2 r_d^{2l-2}}. \tag{13}$$

On the opposite, when $a/A \to 0$, nanoshell spherelike modes reduce to their solid sphere analogues. In particular, their effective volumes [see Eq. (10)] tend to the values

$$V_{\mathrm{sph},l} = \frac{4\pi r_d^{2l+4}}{(l+1)^2 A^{2l+1}}, \tag{14}$$

which perfectly coincide with the effective volumes provided in Ref. 61 for a metallic spherical nanoparticle.

Here, we briefly analyze similarities and differences between nanoshells and their ideal limits: cavities and solid spheres. The natural choice is to compare the nanoshell modes with the ideal cavity ones when the dipole is inside the shell, and with the sphere ones when the dipole is outside. This is corroborated by the fact that, according to Eq. (10), $V_{\mathrm{eff},l}$ is proportional to the inner cavity volume, if the dipole is inside the shell, or to the total volume, if the dipole is outside. Therefore plasmonic modes in small geometries tend to couple better with radiation, being the strength of the coupling roughly proportional to the inverse effective volume [see Eq. (11)].

The main peculiarity of nanoshell plasmonic modes is their additional relation to the shell thickness, or, equivalently, to the ratio a/A. Figure 4(a) shows the ratio between the effective volumes of a cavity [see Eq. (13)] and a nanoshell [see Eq. (10)] as a function of the ratio a/A for a fixed inner radius a. The dipole is situated inside the inner cavity; its distance r_d from the center is kept fixed, too, together with the order l; thus, from the physical point of view, the curve gives a measure of the coupling strength of nanoshell plasmonic modes relatively to the corresponding ideal cavity ones. As can be easily expected, in the limit of large thickness (left area of the plot), cavity-like nanoshell modes are roughly equivalent to the ideal ones, whereas spherelike modes are strongly inhibited. However, when the thickness decreases, spherelike modes become the most favorable in the nanoshell, reaching, in the case of very small thickness, the same order of magnitude of ideal ones.

This behavior is very different from the situation where the dipole is outside the nanoshell [see Fig. 4(b)]. In this second case, as already pointed out, the natural analog is provided by the plasmonic modes of a solid sphere. The ratio between the effective volumes of an ideal sphere [see Eq. (14)] and a nanoshell is displayed in Fig. 4(b), keeping constant the outer radius A, the dipole position r_d, and the order l. As can be seen, in this case, spherelike modes are always the most advantageous ones, irrespective of the shell thickness.

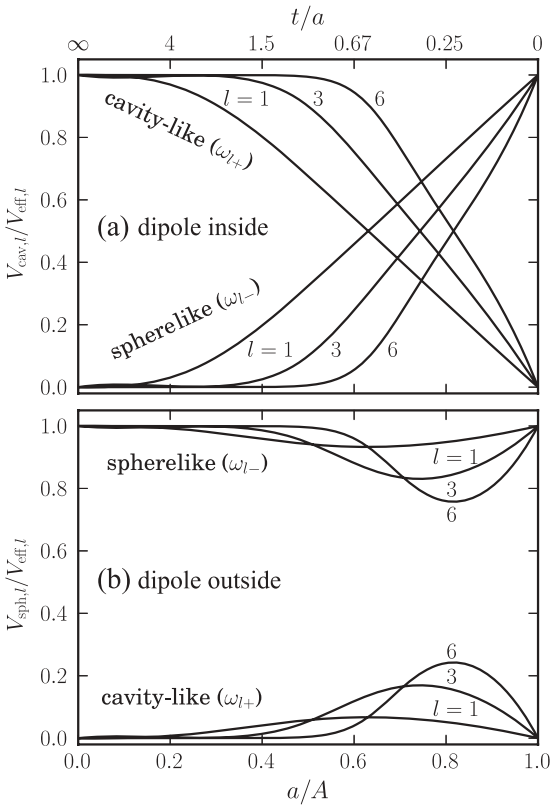

FIG. 4. (a) The ratio between the effective volume of ideal cavity plasmonic modes [see Eq. (13)] and nanoshell ones [see Eq. (10)] versus the nanoshell a/A parameter, calculated at the same order l and for a fixed inner radius a. The dipole is inside the cavity and the ratio is independent of its position. The upper curve refers to the ω_{l+} modes, the lower one to the ω_{l-} modes. For clarity, a thickness scale $[t/a = (A-a)/a]$ has been reported on the upper axis. (b) As above, except that the dipole is outside the outer surface, the outer radius A is kept fixed, and the comparison is with the modes of a solid metallic sphere [see Eq. (14)]. Notice that here the upper curve refers to the ω_{l-} modes, the lower one to the ω_{l+} ones.

The phenomenon is well exemplified by the plots in Fig. 5, displaying the normalized decay rate of a dipole inside and outside a nanoshell for the ratios $a/A = 0.5$ and 0.8. They were obtained from Eq. (11). When the dipole is inside the shell, the coupling with spherelike modes prevails for a sufficiently thin shell; when it is outside, the coupling with cavity-like modes, even if partially enhanced, never becomes significant. A comparison with the retarded solution is presented in Ref. 60 and it shows very good agreement.

With reference to the coupling strength, notice that the value of the curves in Fig. 4 is always less than unity. It means that nanoshell modes are always *disadvantageous* when we compare them to the ideal cavity analogues, if the dipole is inside, or to the solid sphere analogues, if it is outside. However, the previous considerations suggest that a thin nanoshell *with the dipole inside the inner cavity* could also compete with a similarly sized solid sphere, as they share the same plasmon frequency range. Indeed, in many cases, this specific nanoshell arrangement facilitates a stronger coupling with radiation, as it will be elaborated in the following sections, with particular reference to non-Markovian effects.

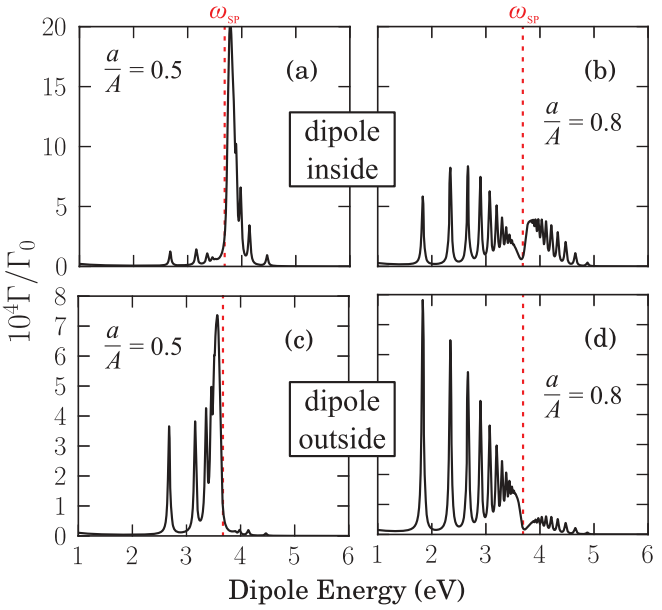

FIG. 5. (Color online) The dipole total decay rate $\Gamma(\omega)$ in the classical approximation [see Eq. (11)] for a silver nanoshell, normalized to the free-space decay rate $\Gamma_0(\omega)$ as a function of the dipole frequency. The parameters are (a) $a = 10$ nm, $A = 20$ nm, $r_d = 8$ nm; (b) $a = 10$ nm, $A = 12.5$ nm, $r_d = 8$ nm; (c) $a = 5$ nm, $A = 10$ nm, $r_d = 12.5$ nm; (d) $a = 8$ nm, $A = 10$ nm, $r_d = 12.5$ nm. The dielectric function follows a Drude model with the parameters in Eq. (4). The vertical dotted red lines indicate the surface plasmon frequency ω_{SP}. In (a) and (b) the dipole is inside the nanoshell, while in (c) and (d), it is outside; moreover, to simplify the comparison with Fig. 4, the plots in the same column share the same a/A ratio (0.5 and 0.8, respectively).

III. STRONG LIGHT-MATTER COUPLING EFFECTS

A. General theory of the emitted-light spectrum

As shown in Refs. 7 and 8, the electric-field operator in a system containing absorptive and dispersive media can be expanded onto a continuous set (both in frequency and space) of bosonic operators $\mathbf{f}(\boldsymbol{r},\omega)$, according to the relations

$$\mathbf{E}(\boldsymbol{r}) = \mathbf{E}^{(+)}(\boldsymbol{r}) + \mathbf{E}^{(-)}(\boldsymbol{r}), \tag{15}$$

$$\mathbf{E}^{(+)}(\boldsymbol{r}) = \int_0^\infty d\omega \underline{\mathbf{E}}(\boldsymbol{r},\omega), \quad \mathbf{E}^{(-)}(\boldsymbol{r}) = [\mathbf{E}^{(+)}(\boldsymbol{r})]^\dagger, \tag{16}$$

$$\underline{\mathbf{E}}(\boldsymbol{r},\omega) = i\frac{\omega^2}{c^2}\sqrt{\frac{\hbar}{\pi\epsilon_0}} \times \int d\boldsymbol{r}'\sqrt{\mathrm{Im}\,\epsilon(\boldsymbol{r}',\omega)}\ \overleftrightarrow{G}(\boldsymbol{r},\boldsymbol{r}',\omega)\cdot\mathbf{f}(\boldsymbol{r}',\omega), \tag{17}$$

where $\overleftrightarrow{G}(\boldsymbol{r},\boldsymbol{r}',\omega)$ is the electric dyadic Green function.

Considering a dipole with frequency ω_d located at the point $\boldsymbol{r}_d$ in vacuum, its interaction with radiation is described in terms of the Pauli operators $\sigma^{(\pm)}$ and the transitional dipole moment $\boldsymbol{\mu}$, by means of the rotating-wave approximated Hamiltonian

$$H_{\mathrm{int}} = -[\sigma^{(-)}\mathbf{E}^{(+)}(\boldsymbol{r}_d)\cdot\boldsymbol{\mu} + \mathrm{H.c.}]. \tag{18}$$

The state of the system can be expanded onto the dipole ground and excited states—|gr⟩ and |ex⟩—and the unperturbed

eigenstates $|n_{j,\boldsymbol{r},\omega}\rangle$ of the number operator $\mathrm{f}_j^\dagger \mathrm{f}_j(\boldsymbol{r},\omega)$:

$$|\psi(t)\rangle = C(t)e^{-i\frac{1}{2}\omega_d t}\,|\mathrm{ex}\rangle\,|0\rangle + \int d\boldsymbol{r}\int_0^\infty d\omega\, D_{j,\boldsymbol{r},\omega}(t)e^{-i(\omega-\frac{1}{2}\omega_d)t}\,|\mathrm{gr}\rangle\,|1_{j,\boldsymbol{r},\omega}\rangle\,. \tag{19}$$

The coefficients must be calculated from the Schrödinger equation, which, in the case of $C(t)$, assumes the form

$$\dot{C}(t) = \int_0^t dt' K(t-t')C(t'), \tag{20}$$

$$\text{with}\quad K(\tau) = -\int_0^\infty d\omega \frac{\omega^2}{\hbar\pi\epsilon_0 c^2} e^{-i(\omega-\omega_d)\tau} \times \boldsymbol{\mu}\cdot \mathrm{Im}\,\overleftrightarrow{G}(\boldsymbol{r}_d,\boldsymbol{r}_d,\omega)\cdot\boldsymbol{\mu}. \tag{20}$$

The light intensity spectrum of the radiation spontaneously emitted by the dipole (without external driving), registered by an ideal detector at a point $\boldsymbol{r}$ sufficiently away from the source, can be defined as

$$S(\boldsymbol{r},\omega) = \frac{2\epsilon_0 c}{2\pi}\int_0^\infty dt_2 \int_0^\infty dt_1\, e^{-i\omega(t_2-t_1)} \times \langle \mathbf{E}^{(-)}(\boldsymbol{r},t_2)\cdot\mathbf{E}^{(+)}(\boldsymbol{r},t_1)\rangle\,. \tag{21}$$

Still according to Ref. 7, the previous expression becomes

$$S(\boldsymbol{r},\omega) = \frac{\epsilon_0 c}{\pi}\sum_j \left| \int_0^\infty dt\, e^{i(\omega-\omega_d)t}\int_0^t dt'\, C(t') \times \int_0^\infty d\omega' \frac{\mu_n(\omega')^2}{\pi\epsilon_0 c^2}\,\mathrm{Im}\,\overleftrightarrow{G}_{jn}(\boldsymbol{r},\boldsymbol{r}_d,\omega')\,e^{-i(\omega'-\omega_d)(t-t')}\right|^2. \tag{22}$$

This formula can be expressed in an equivalent form, by observing that the term in the absolute square is the Laplace transform, calculated at the point $i(\omega_d-\omega)$, of the Laplace convolution of the two functions. Then, it can be replaced with the product of their Laplace transforms:

$$S(\boldsymbol{r},\omega) = \frac{\epsilon_0 c}{\pi}\sum_j |F_j(\boldsymbol{r},\boldsymbol{r}_d,\omega)|^2\,|\mathcal{L}[C][i(\omega_d-\omega)]|^2, \tag{23}$$

where the function $F_j(\boldsymbol{r},\boldsymbol{r}_d,\omega)$ is introduced in Ref. 7 as

$$F_j(\boldsymbol{r},\boldsymbol{r}_d,\omega) = \frac{\mu_n}{\pi\epsilon_0 c^2}\int_0^\infty d\omega'\,(\omega')^2 \mathrm{Im}\,\overleftrightarrow{G}_{jn}(\boldsymbol{r},\boldsymbol{r}_d,\omega') \times\left[\pi\delta(\omega-\omega') + i\mathcal{P}\frac{1}{\omega-\omega'}\right]. \tag{24}$$

Referring to the same work, we remind that the quantity

$$I(\boldsymbol{r},\omega) = 2\epsilon_0 c\sum_j |F_j(\boldsymbol{r},\boldsymbol{r}_d,\omega)|^2 \tag{25}$$

represents the intensity of the light emitted towards a point $\boldsymbol{r}$ by a hypothetical dipole with energy $\hbar\omega$, calculated in the classical (Markov) approximation. The second term in Eq. (23) can be evaluated recalling that the Schrödinger integrodifferential equation (20) simply reduces to an algebraic equation when Laplace transformed:

$$\mathcal{L}[C](s) = \frac{C(0)}{s-\mathcal{L}[K](s)} = \frac{1}{s-\mathcal{L}[K](s)}. \tag{26}$$

We define the quantum efficiency $\eta_{\mathrm{rad}} = \Gamma_{\mathrm{rad}}/\Gamma$, with Γ_{rad} being the ratio between the far-field emitted power and the dipole energy, and notice that the emitted power can be expressed as the integral of Eq. (25) over the solid angle, in the limit $\boldsymbol{r}\to\infty$. Then, the integral of Eq. (23) over the solid angle can be identified with the radiated power spectrum:

$$S(\omega) = \int d\Omega \lim_{r\to\infty} r^2 S(\boldsymbol{r},\omega) = \frac{\hbar\omega}{2\pi}\eta_{\mathrm{rad}}(\omega)\Gamma(\omega)\left|\frac{1}{i(\omega_d-\omega)-\mathcal{L}[K](i\omega_d-i\omega)}\right|^2. \tag{27}$$

Equation (27) expresses the radiated power spectrum as the product of the dipole energy, the radiative decay rate, and the line-shape function.

If we recall the definition[7] of the generalized Lamb shift

$$\delta\omega(\omega) = \frac{1}{\pi\hbar\epsilon_0 c^2}\mathcal{P}\int_0^\infty d\omega'\,(\omega')^2\,\frac{\boldsymbol{\mu}\cdot\mathrm{Im}\,\overleftrightarrow{G}(\boldsymbol{r}_d,\boldsymbol{r}_d,\omega')\cdot\boldsymbol{\mu}}{\omega'-\omega}, \tag{28}$$

the Laplace transform of the kernel $\mathcal{L}[K](s)$ can be simplified to the form [see also Eq. (12)]

$$\mathcal{L}[K][i(\omega_d-\omega)] = -\tfrac{1}{2}\Gamma(\omega) + i\delta\omega(\omega). \tag{29}$$

By replacing it into Eq. (27), we obtain

$$S(\omega) = \frac{\hbar\omega}{2\pi}\eta_{\mathrm{rad}}(\omega)\Gamma(\omega)\left|\frac{1}{i[\omega_d-\omega-\delta\omega(\omega)]+\frac{1}{2}\Gamma(\omega)}\right|^2; \tag{30}$$

this is the rotating-wave approximated version of the result reported in Ref. 63 and allows to calculate the emitted-light spectrum whenever analytical expressions of the classical decay rate and Lamb shift are known. Notice that the equation makes it possible to study nonperturbative effects, although the decay rate $\Gamma(\omega)$ is calculated by means of the Fermi golden rule.

When the intensity of the coupling is weak, by approximating all the slowly-varying terms with their central value at ω_d and renormalizing the dipole frequency to include the Lamb shift, we recover the expected Lorentzian-shaped power spectrum:

$$S(\omega) = \frac{1}{\pi}\eta_{\mathrm{rad}}(\omega_d)\hbar\omega_d\frac{\frac{1}{2}\Gamma(\omega_d)}{(\omega-\omega_d)^2+\left[\frac{1}{2}\Gamma(\omega_d)\right]^2}, \tag{31}$$

which is correctly normalized to the overall energy radiated by the dipole,

$$\int d\omega\, S(\omega) = \eta_{\mathrm{rad}}(\omega_d)\hbar\omega_d. \tag{32}$$

B. Case of a Lorentzian-shaped dipole decay rate

In this section, we apply the general theory of Sec. III A to treat the crossover between weak and strong coupling regimes. In particular, we consider the situation in which the perturbative decay rate can be expanded onto a sum of Lorentzian functions. Let us suppose, for the moment, that it consists of a single Lorentzian function of the form

$$\Gamma(\omega) = \Gamma(\omega_0)\frac{\left(\frac{1}{2}\gamma\right)^2}{(\omega-\omega_0)^2+\left(\frac{1}{2}\gamma\right)^2}. \tag{33}$$

Then, the kernel $K(\tau)$, defined in Eq. (20), reduces to an elementary Fourier transform and can be worked out to obtain

$$K(\tau) = -\tfrac{1}{4}\Gamma(\omega_0)\gamma e^{i(\omega_d-\omega_0)\tau-\frac{1}{2}\gamma|\tau|}. \tag{34}$$

In the calculation, the ω integral has been extended from $-\infty$ to ∞, on the base that within the rotating-wave approximation, the two integrals are the same.[64] Upon performing the Laplace transform, we obtain

$$\mathcal{L}[K](s) = -\frac{1}{4}\,\frac{\Omega^2}{s+\frac{1}{2}\gamma-i(\omega_d-\omega_0)}, \tag{35}$$

where we have introduced the *Rabi frequency* $\Omega = \sqrt{\Gamma(\omega_0)\gamma}$.

To underline the physical meaning of the expression, let us suppose that the dipole is resonant with the Lorentzian function, i.e., $\omega_d = \omega_0$. Having defined $\Delta = \sqrt{\frac{1}{4}\gamma^2-\Omega^2}$, the substitution of Eq. (35) in Eq. (27) leads to

$$S(\omega) = \frac{\hbar\omega}{2\pi}\eta_{\mathrm{rad}}(\omega)\Gamma(\omega) \times \frac{1}{4}\left|\frac{1+\frac{\gamma}{2\Delta}}{s+\frac{1}{4}\gamma-\frac{1}{2}\Delta}+\frac{1-\frac{\gamma}{2\Delta}}{s+\frac{1}{4}\gamma+\frac{1}{2}\Delta}\right|^2_{s=i(\omega_d-\omega)}. \tag{36}$$

When $\Omega^2 < \frac{1}{4}\gamma^2$, the spectrum is single-peaked around the frequency ω_0; in particular, if $\gamma \gg \Omega$, we recover the weak coupling result of the previous section; however, when $\Omega^2 > \frac{1}{4}\gamma^2$, the term Δ becomes purely imaginary, and the spectrum splits into a doublet of peaks separated by $\mathrm{Im}(\Delta)$, giving rise to the well-known phenomenon of *Rabi splitting*. Notice that, if $\Omega \gg \gamma$, the doublet splitting approaches Ω.

As a consequence, the condition for the establishment of a Rabi splitting in the emission spectrum can be written as $\gamma^2 < 4\Omega^2$, i.e., $\gamma < 4\Gamma(\omega_0)$. It depends only on the dipole *total* decay rate in the classical approximation and it does not discriminate between radiative and nonradiative processes. Thus, in many systems, the strong coupling regime could be entered due to a contribution from the nonradiative coupling, in spite of the radiative component alone being insufficient.

This is obviously the case of small nanoshells, where we have seen that the huge enhancement of the classical decay rate is mainly of nonradiative origin. As a starting point, we suppose that the dipole is in interaction with a single plasmonic mode and neglect the contribution from the free-space decay and all the other modes. Equation (11) becomes

$$\Gamma(\omega) = \frac{2\mu^2\omega_{l\pm}}{\hbar\epsilon_0\gamma_{\mathrm{D}}}V^{-1}_{\mathrm{eff},l}\,\frac{\left(\frac{1}{2}\gamma_{\mathrm{D}}\right)^2}{(\omega-\omega_{l\pm})^2+\left(\frac{1}{2}\gamma_{\mathrm{D}}\right)^2}. \tag{37}$$

Recalling that the dipole *oscillator strength* is defined as $f = 2m_e\omega_d\mu^2/(e^2\hbar)$, when the dipole is resonant with $\omega_{l\pm}$, the Rabi frequency Ω is seen to coincide with twice the coupling constant g of the dipole-cavity interaction introduced in Ref. 65:

$$\Omega = 2g = \sqrt{\frac{e^2 f}{m_e\epsilon_0 V_{\mathrm{eff},l}}}. \tag{38}$$

Analogously, the emission spectrum in Eq. (36) reduces to a cavity-QED result obtainable with a master-equation approach.[65,66]

The Rabi-splitting condition $\gamma_{\mathrm{D}}^2 < 4\Omega^2$ discussed above can be recast in the form $f > f_{\mathrm{th}}$, where f_{th} is the threshold oscillator strength for entering the strong coupling regime:

$$f_{\mathrm{th}} = \frac{m_e\gamma_{\mathrm{D}}^2\epsilon_0 V_{\mathrm{eff},l}}{4e^2}. \tag{39}$$

In our model, the threshold oscillator strength is proportional to the effective volume; since we have obtained its analytical expression, we can easily deduce which is the most advantageous plasmonic mode for every choice of the geometrical parameters of the system. Notice that f_{th} grows quadratically with the metal dissipation.

The threshold oscillator strength provides guidance on the intensity of the Rabi-splitting phenomena; however, in order to calculate the emission spectrum, we cannot neglect the contribution from the remaining plasmonic modes; in addition, we are interested also in the case when the dipole is not in resonance with any particular mode. The expression for the spectrum can be generalized to the full decay rate in Eq. (11) by combining the previous results (29) and (35) via linearity:

$$S(\omega) = \frac{\hbar\omega}{2\pi}\eta_{\mathrm{rad}}(\omega)\Gamma(\omega)\left|i(\omega_d-\omega)+\frac{1}{2}\Gamma_0(\omega) + \sum_l\left(\frac{\omega_{l\pm}e^2 f}{4\omega_d m_e\epsilon_0}\right)\frac{V^{-1}_{\mathrm{eff},l}}{\frac{1}{2}\gamma_l-i(\omega-\omega_{l\pm})}\right|^{-2}. \tag{40}$$

This result has already been obtained in the context of cavity quantum electrodynamics.[67] Equation (40) is equivalent to Eq. (30) and contains the resonant contributions to the Lamb shift in the last term ($\sum_l \ldots$). This holds because the classical decay rate $\frac{1}{2}\Gamma(\omega)$ and the Lamb shift $\delta\omega(\omega)$ are related by the Kramers–Kronig relations [compare Eqs. (12) and (28)]. In Eq. (40), the Lamb shift is not an independent quantity, being determined by the additional assumption on the Lorentzian shape of the classical decay rate.

The term $\eta_{\mathrm{rad}}(\omega)\Gamma(\omega)$ in Eq. (40) keeps track of the light propagation from the dipolar source to the detector; in this work, however, we are mainly interested in the conditions for entering a strong coupling regime, which depend only on the dipole local dynamics and are entirely included in the absolute square term. For this reason, we will generally concentrate only on the latter and, for clarity, call it the

dipole spectrum:

$$P(\omega) = \left| i(\omega_d - \omega) + \frac{1}{2}\Gamma_0(\omega) + \sum_l \left(\frac{\omega_{l\pm} e^2 f}{4\omega_d m_e \epsilon_0} \right) \frac{V_{\mathrm{eff},l}^{-1}}{\frac{1}{2}\gamma_l - i(\omega - \omega_{l\pm})} \right|^{-2}. \quad (41)$$

Notice that, being the quantum efficiency term calculated at the detector frequency (not at the dipole one), it can cause some distortion onto the detected spectrum; in particular, it can give rise to some spurious peaks due to low-coupling but high-radiative modes, as shown in Ref. 50 in the case of spherical particles.

C. Optimization of nanoshell parameters towards the Rabi-splitting regime

Equation (39) provides a threshold condition for the formation of a Rabi splitting in the emitted light spectrum of a dipole resonant with a nanoshell plasmonic mode, when the dielectric function follows the Drude model. The resonance frequency depends on the choice of the mode and on the geometry. Usually, however, we are interested in the opposite problem, i.e., to find the parameters that maximize the coupling with radiation for a fixed-frequency dipole. Under the condition of a fixed dipole moment, the fact that the effective volume scales as a^3 or A^3 [see Eq. (10)] suggests at first to minimize the geometrical extension of the system; in addition, the local coupling is enhanced with the decreasing of the distance between the dipole and the nearest metallic surface.

The selection of the best value for the shell thickness, or, equivalently, for the ratio a/A, requires some elaboration. By inverting Eq. (5), we can calculate a set of pairs $(\frac{a}{A},l)$ satisfying the relation

$$\left(\frac{a}{A}\right)^{2l+1} = \frac{(2l+1)^2\left[2\left(\frac{\omega_d}{\omega_P}\right)^2 - 1\right]^2 - 1}{4l(l+1)}. \quad (42)$$

Each pair corresponds to a plasmonic mode with the frequency coinciding with the dipole one. In this set, we can identify the optimal mode that minimizes the effective volume, characterized by the parameters $(\frac{a}{A},l_{\mathrm{opt}})$: the two quantities are displayed in Figs. 6 and 7 by the dashed line in (a) and the solid line in (b), respectively. The solid line in Figs. 6(a) and 7(a), instead, represents the corresponding minimal effective volume (normalized with respect to a^3, in Fig. 6, or A^3, in Fig. 7). The effective volume can be used to calculate the threshold oscillator strength according to Eq. (39). For instance, in the case of silver [with the Drude damping constant in Eq. (4)], the quantity $m_e\gamma_D^2\epsilon_0/(4e^2)$ is equal to 3.51×10^{-4} nm^{-3}.

As an example of application, we suppose to have a dipole with a frequency of approximately 2.9 eV–as in Ref. 51—coupled to a silver nanoshell [see Eq. (4)], which gives $\omega_d/\omega_P = 0.56$. If the dipole is located inside the inner cavity of a nanoshell, from Fig. 6(b) we deduce that the best-coupling mode is the fifth spherelike one, while the dashed line in Fig. 6(a), provides us with the ratio $a/A \simeq 0.83$. The dipole spectrum for a nanoshell with inner radius of 10 nm is shown for several values of the dipole oscillator strength in Fig. 8(a);

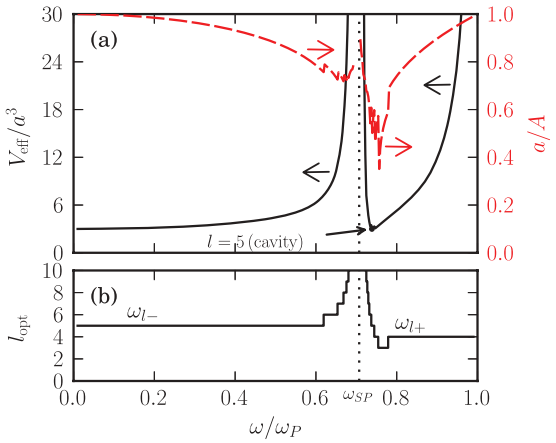

FIG. 6. (Color online) Selecting the parameters that optimize the coupling with radiation for a fixed-frequency radially oriented dipole, located inside the inner cavity of a metallic nanoshell at a distance $0.8a$ from the center. (a) Solid line: the effective volume (normalized to a^3) of the plasmonic mode that optimizes the coupling, as a function of the dipole frequency (normalized to ω_P). Dashed red line: the ratio a/A necessary to make the optimal-mode frequency coincident with the dipole one. (b) The order of the optimal mode. If the dipole frequency is larger than ω_{SP}, it is understood that we refer to cavity-like modes, otherwise to spherelike ones.

notice that the splitting is compatible with the estimate of the threshold oscillator strength provided by Fig. 6(a), which is of the order of two. Similarly, an analysis of Fig. 7 suggests that, when the dipole is outside the sphere, the best coupling is achieved with the $l = 3$ spherelike mode of a nanoshell with ratio $a/A \simeq 0.75$. Figure 8(b) shows an example of the dipole spectrum for a nanoshell with $A = 10$ nm. In this case, the Rabi splitting occurs at higher values of the oscillator strength, in agreement with the threshold estimated from Fig. 7(a), of the order of three.

In can be observed from Fig. 6 that, when the dipole frequency happens to coincide with a bare cavity resonance [see Eq. (8)], there is a large drop in the value of the optimal a/A ratio; in these cases, then, the best coupling is achieved

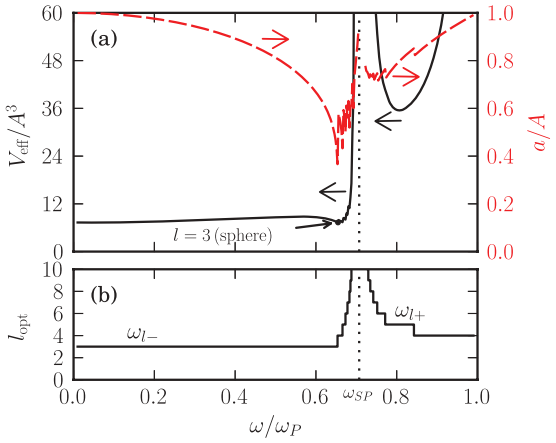

FIG. 7. (Color online) Analogue to Fig. 6, except that in this case the dipole is outside the outer surface at the position $r_d = A/0.8$ and the effective volume is normalized to A^3 instead of a^3. This last difference must be taken into consideration when applying Eq. (39).

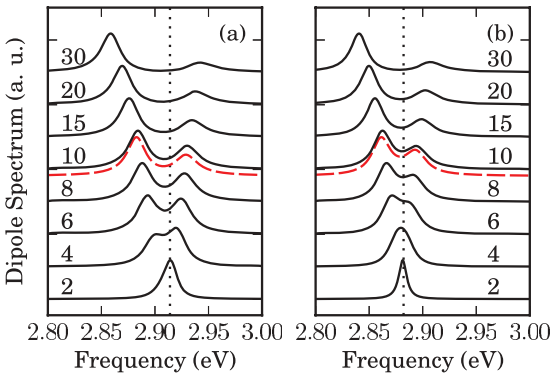

FIG. 8. (Color online) Solid curves: dipole (polarization) spectrum of a radial dipole in proximity to a silver nanoshell, for several values of the dipole oscillator strength (indicated by the numbers on curves), calculated with Eq. (41). The dielectric function follows the Drude model [see Eq. (4)] and each curve is normalized independently of the others. Parameters are (a) $a = 10$ nm, $A = 12$ nm, $r_d = 8$ nm, dipole frequency of 2.91 eV (dotted vertical line); (b) $a = 7.5$ nm, $A = 10$ nm, $r_d = 12.5$ nm, dipole frequency of 2.88 eV. As a comparison, in the case $f = 10$, the additional red dashed curve represents the dipole spectrum including retardation effects, calculated with Eq. (27) and the exact expression for the dyadic Green function provided in Ref. 20. It is normalized independently of the quasistatic one and slightly shifted for better clarity.

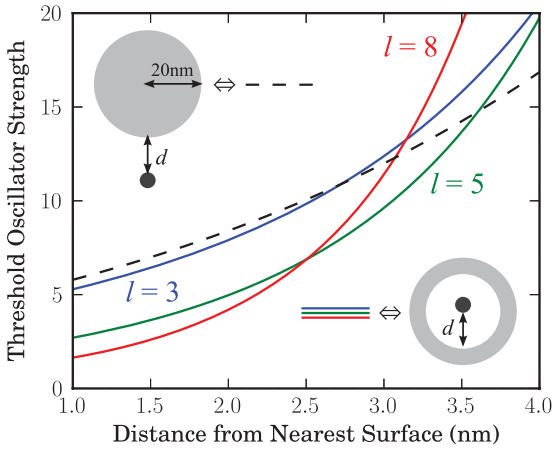

FIG. 9. (Color online) Dashed line: threshold oscillator strength to enter the strong coupling regime for a dipole near a silver nanosphere with radius of 20 nm as a function of the distance d from the metal surface (see upper left inset). The dipole is resonant with the second plasmonic mode, at the frequency $\omega_{\rm sph} = \sqrt{\frac{2}{5}}\omega_{\rm P}$ [see Eq. (7)]. Solid lines: threshold oscillator strengths for a dipole located in vacuum inside a silver nanoshell with the same outer radius $A = 20$ nm, as a function of the distance from the inner metallic surface (see lower right inset). The dipole is in resonance with a nanoshell spherelike mode of the order l indicated on the curves; the thickness is chosen according to Eq. (42) to make the modal frequency ω_{l-} coincident with ω_d.

when the geometry of the system approaches that of an ideal cavity. For better clarity, we have added an arrow in the plot indicating the frequency and the normalized effective volume of the ideal cavity best resonance. An analogous phenomenon is shown in Fig. 7, where the arrow indicates the best coupling mode of a solid sphere. In agreement with our previous considerations, we see that the minimal threshold oscillator strength for nanoshells is of the same order of that for ideal cavities when the dipole is inside, and of that for solid spheres when it is outside. However, a clear advantage of the nanoshell geometry is the possibility to tune the best-coupling frequency over a large range of the frequency spectrum by regulating the shell thickness, at variance from the case of particles and cavities, which are characterized by fixed modal frequencies.

D. Comparison of shell and single-particle geometries

In Sec. II, we have compared the behavior of a dipole in proximity to a spherical particle with that of a dipole outside the external surface of a metallic nanoshell. It turns out that, for a given l and total radius, in the nanoshell geometry the dipole couples less with radiation than in the particle geometry, as shown particularly in Fig. 4(b). However, we have also observed from Fig. 4(a) that, when the dipole is *inside* the inner surface, nanoshells present an interesting "inversion" phenomenon in the relative strength of spherelike and cavity-like modes: if the shell thickness is sufficiently low, the coupling with spherelike modes greatly overcomes that with cavity-like modes. At the same time, the dipole frequency range most suitable to decay rate enhancement moves to the $\omega < \omega_{\rm SP}$ region of the spectrum, overlapping with the resonances of a single metallic sphere. This behavior suggests us to compare the solid-particle geometry with the case of a dipole inside the inner cavity of a nanoshell. If the shell thickness is low enough, the latter choice could provide an easier way to reach the strong coupling regime.

In order to be meaningful, the comparison must be drawn for the same dipole frequency. Let us suppose, for instance, that the dipole is in resonance with the second surface plasmon of a particle, at the frequency $\omega_d = \sqrt{\frac{2}{5}}\omega_{\rm P}$ [see Eq. (7)]. From Eq. (42), we deduce that, for every integer $l > 2$, there exists a value of the ratio a/A that makes the lth plasmon frequency ω_{l-} coincident with ω_d. In general, this ratio implies a progressively smaller thickness of the shell on the increase of the modal order l. We clearly refer to the spherelike plasmonic modes, whose frequencies ω_{l-} are always below the surface plasmon threshold $\omega_{\rm SP}$ and share the same range with particle resonances. The corresponding threshold oscillator strength can be obtained from Eq. (39) and is plotted in Fig. 9 as a function of the distance from the metal surface. As can be seen, when the distance is sufficiently small, this particular nanoshell arrangement can provide a more advantageous threshold to the strong coupling regime than a particle with radius equal to A.

Figure 10 provides an example of such behavior. In Figs. 10(a) and 10(b), we plot the semiclassical decay rate for a dipole inside a silver nanoshell (a) and outside a silver particle (b), as a function of the dipole frequency. The nanoshell has parameters $A = 20$ nm and $a = 16.46$ nm, which, according to Eq. (5), set the frequency of the $l = 8$ ω_{l-} mode perfectly coincident with the $l = 2$ particle mode, at $\omega_{\rm sph} = \sqrt{\frac{2}{5}}\omega_{\rm P} = 3.29$ eV (indicated by the vertical dotted lines). We are interested in dipole frequencies in proximity to $\omega_{\rm sph}$. In the case of the particle (b), there is a small peak

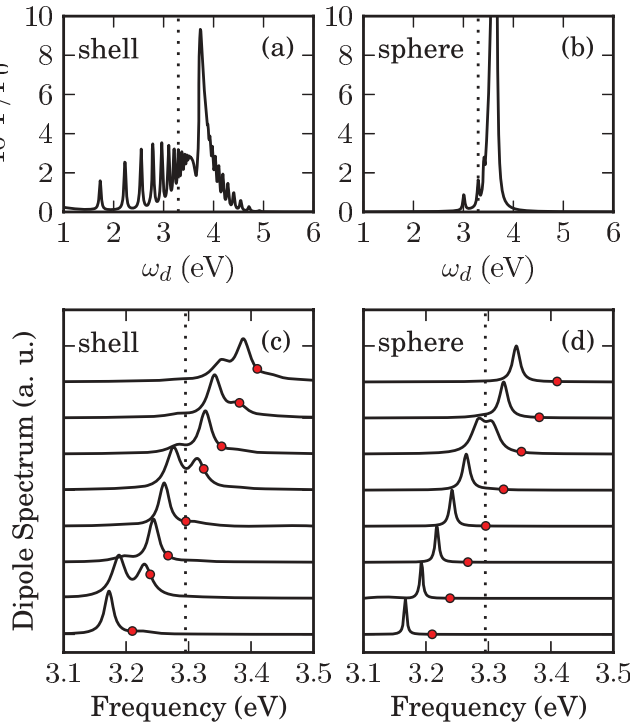

FIG. 10. (Color online) The semiclassical decay rate of a radial dipole in proximity (a) to a silver nanoshell with parameters $A = 20$ nm, $a = 16.46$ nm, $r_d = 14.46$ nm; (b) to a silver nanosphere with parameters $A = 20$ nm, $r_d = 22$ nm, calculated with the Purcell equation (11). The dipole is 2 nm away from the inner surface [in (a)], or the sphere surface [in (b)]; it is characterized by an oscillator strength of 20. Frame (c) for the nanoshell and frame (d) for the sphere show the dipole (polarization) spectra obtained with Eq. (41) for several values of the dipole frequency, which are indicated by the superimposed red dots; they include the contributions from all the plasmonic modes of the system and each curve is normalized independently of the others. The frequency 3.29 eV (indicated by vertical dotted lines) characterizes both the $l = 8$ spherelike ω_{l-} mode of the nanoshell and the $l = 2$ mode of the sphere: as a typical consequence of the strong coupling regime, there is a Rabi splitting phenomenon when the dipole frequency is in its proximity.

centered on $\omega_{\rm sph}$ in the semiclassical decay rate: consequently, the dipole spectrum presents a slightly noticeable Rabi splitting phenomenon when the dipole frequency ω_d approaches $\omega_{\rm sph}$. On the other hand, in the case of the nanoshell (a), the peak centered on $\omega_{\rm sph}$ is far higher, giving rise to an easily observable and well defined Rabi splitting for $\omega_d \simeq \omega_{\rm sph}$. This is shown in Figs. 10(c) and 10(d), representing the dipole spectra for the nanoshell and particle geometries, respectively. Each curve has been calculated through Eq. (41) for a different dipole frequency ω_d (indicated by the red dot). Calculated spectra show that when the dipole is inside a nanoshell, the coupling with the spherelike modes is more convenient to the Rabi splitting than when the dipole is outside a solid sphere. Notice that the position of the peaks in the spectra is redshifted with respect to the dipole frequency due to the presence of a large anticrossing centered around the surface plasmon frequency at about 3.7 eV [not shown in Figs. 10(c) and 10(d)], as can be inferred from the presence of a very high peak in both Figs. 10(a) and 10(b).

The presence of Rabi splitting phenomena in the spectrum emitted by a dipole near a spherical particle in particular conditions has been extensively treated in Ref. 50. Here, we additionally state that such behavior can be notably highlighted with a suitable nanoshell arrangement, especially when the dipole is meant to couple with low-frequency and highly radiative particle modes. On the other hand, as a counterpart for the enhanced coupling strength, since in the nanoshell case higher-order modes are involved, a quenching of radiative phenomena is to be expected. This is in agreement with our considerations after Eq. (36), regarding the equivalence of radiative and nonradiative processes in entering the strong coupling regime. In this case, the gain in strength comes mostly from the nonradiative ones.

IV. DISCUSSION AND CONCLUSIONS

We have given a formulation of the interaction between an oscillating dipole and a metal nanoshell, which emphasizes the role of localized surface plasmon resonances for radiation-matter coupling. By adopting the quasistatic approximation (suitable for small nanoshells, which are the most promising ones for control of decay rates and for strong coupling), we have obtained analytical expressions for surface plasmon frequencies and effective volumes, the latter being defined for any position of the dipole inside or outside the nanoshell. The dipole decay rate reflects the full spectrum of modes, which can be classified as spherelike or cavity-like. The effective volume depends strongly on mode order l and on inner and outer radii. In particular, when the dipole is inside the nanoshell, a surprising "inversion" phenomenon occurs: while coupling to cavity-like modes dominates for thick shells, dominant coupling switches to spherelike modes when the shell is thin enough. This has important consequences for the regimes of light-matter interaction.

In the second part of the paper, we have presented a theory of emission spectra beyond the perturbative regime and have studied the conditions for the occurrence of strong, nonperturbative light-matter coupling. The Rabi frequency depends on the total decay rate, thus being unaffected by the radiative efficiency. It depends on the dipole oscillator strength and on the mode effective volume with the same kind of expression that holds for other cavity-QED systems (e.g., for a quantum dot in a photonic cavity).[65] This leads to an expression for the threshold oscillator strength as a function of effective volume and metal dissipation. By optimizing the geometrical parameters of the nanoshell to minimize the effective volume we can determine the optimal conditions for strong coupling, which yield oscillator strengths as low as a few units that can be easily obtained with typical emitters (quantum dots or organic molecules). Furthermore, the "inversion" phenomenon just mentioned implies that a dipole inside a nanoshell and coupled to spherelike modes is more favorable for strong coupling than the same dipole interacting with a full metal sphere of the same total radius, provided that the shell is thin enough to allow the excitation of the dipole and the detection of the emitted radiation.

The present approach based on a decay rate expressed as a sum over surface plasmon resonances could be applied to more complicated geometries requiring numerical determination

of the spectra, provided they can be fitted with Lorentzian functions. When applying the results of this work to specific metallic systems, care should be taken in quantifying the crucial parameter of dissipation, which in the present work is simply modeled by a Drude term: effects related to interband transitions—possibly modifying the spectrum of plasmonic resonances, and/or increasing dissipation—should be taken into account. Moreover, when the dimensions of the system become much smaller than the mean-free path of the electrons, a spatially nonlocal dielectric function could be required.[68–72] Even with these words of caution, metallic nanoshells are promising systems to tailor light-matter interaction with plasmonic resonances, also for demonstrating the strong-coupling regime. The main point is that the degrees of freedom provided by the inner and outer radii can be usefully exploited to tune the frequencies and effective volumes of plasmonic resonances. While we have given examples of "optimal" designs from a theoretical point of view, in a real experiment, the conditions for strong coupling might be met by probing different nanoshells, taking advantage of size distribution. Other mechanisms of *in situ* tuning could be devised, e.g., filling the core of the shell with an easily tunable material.[73] It could also be useful to probe the effective mode volume, or local field enhancement, in the proximity of metal nanostructures by means of near-field optical microscopy.[74–76] Once surface plasmon frequencies, effective volumes, and metal dissipation are known, the threshold oscillator strength for strong coupling can be simply evaluated. This conclusion, which is independent of nanoparticle geometry, should be of help in guiding the search for the nonperturbative regime of light-matter coupling.

ACKNOWLEDGMENTS

The authors are grateful to Dario Gerace for a critical reading of the manuscript. This work was supported by Fondazione Cariplo through project 2010-0523.

APPENDIX: QUASISTATIC APPROXIMATION OF THE EXACT DECAY RATE

The dyadic Green function for an inhomogeneous medium can be split into a free-space term and a scattering term, in the form $\overleftrightarrow{G}(\boldsymbol{r},\boldsymbol{r}',\omega) = \overleftrightarrow{G}^0(\boldsymbol{r},\boldsymbol{r}',\omega) + \overleftrightarrow{G}^s(\boldsymbol{r},\boldsymbol{r}',\omega)$. Here, we will follow closely the notation used in Ref. 53. In the case of a nanoshell, if the dipole is inside the inner cavity, the scattering part of the dyadic Green function takes the form

$$\overleftrightarrow{G}^{s(33)}(\boldsymbol{r},\boldsymbol{r}',\omega) = \frac{ik}{4\pi}\sum_{l=0}^{+\infty}\sum_{m=0}^{l}(2-\delta_{m0})\frac{2l+1}{l(l+1)}\frac{(l-m)!}{(l+m)!}\left[\mathcal{C}_{\mathrm{M}}^{(33)}(\omega)\boldsymbol{M}_{\substack{e\\o}lm}(k,\boldsymbol{r})\boldsymbol{M}_{\substack{e\\o}lm}(k,\boldsymbol{r}') + \mathcal{C}_{\mathrm{N}}^{(33)}(\omega)\boldsymbol{N}_{\substack{e\\o}lm}(k,\boldsymbol{r})\boldsymbol{N}_{\substack{e\\o}lm}(k,\boldsymbol{r}')\right], \quad \text{(A1)}$$

on the other hand, if the dipole is beyond the outer surface, it reads

$$\overleftrightarrow{G}^{s(11)}(\boldsymbol{r},\boldsymbol{r}',\omega) = \frac{ik}{4\pi}\sum_{l=0}^{+\infty}\sum_{m=0}^{l}(2-\delta_{m0})\frac{2l+1}{l(l+1)}\frac{(l-m)!}{(l+m)!}\left[\mathcal{B}_{\mathrm{M}}^{(11)}(\omega)\boldsymbol{M}_{\substack{e\\o}lm}^{(1)}(k,\boldsymbol{r})\boldsymbol{M}_{\substack{e\\o}lm}^{(1)}(k,\boldsymbol{r}') + \mathcal{B}_{\mathrm{N}}^{(11)}(\omega)\boldsymbol{N}_{\substack{e\\o}lm}^{(1)}(k,\boldsymbol{r})\boldsymbol{N}_{\substack{e\\o}lm}^{(1)}(k,\boldsymbol{r}')\right], \quad \text{(A2)}$$

where we indicate with the superscript "(1)" the substitution of the spherical Bessel functions with the corresponding Hankel functions of the first kind. The definitions of the wave vectors and the coefficients are provided in Ref. 53 and we will not report them here. The dipole total decay rate $\Gamma(\omega)$ is related to the imaginary part of the dyadic Green function by Eq. (12).

The quasistatic approximation consists of taking the limit $c \to \infty$ of the total decay rate. This can be accomplished by considering the first term of the power series expansion of the Bessel and Hankel functions in Eqs. (A1) and (A2). If the metal dielectric function follows a Drude model, we obtain

$$\frac{\Gamma(\omega)}{\Gamma_0(\omega)} \simeq 1 + \sum_{l\geqslant 1} G_l(\omega), \quad \text{(A3)}$$

where, in the case of a radially oriented dipole inside the inner cavity,

$$G_l(\omega) = 3\frac{l^2(l+1)}{2l+1}\frac{r_d^{2l-2}}{k^3}\frac{\gamma_{\mathrm{D}}\,\omega\,\omega_{\mathrm{P}}^2\left(\omega^2-\frac{l}{2l+1}\omega_{\mathrm{P}}^2\right)\left(\omega^2-\frac{1}{2}\omega_{\mathrm{P}}^2\right)}{\left(\omega^2-\omega_{l+}^2\right)^2\left(\omega^2-\omega_{l-}^2\right)^2+\gamma_{\mathrm{D}}^2\omega^2\left(2\omega^2-\omega_{\mathrm{P}}^2\right)^2}\left(\frac{1}{a^{2l+1}}-\frac{1}{A^{2l+1}}\right), \quad \text{(A4)}$$

otherwise, if the dipole is outside the shell,

$$G_l(\omega) = 3\frac{l(l+1)^2}{2l+1}\frac{1}{r_d^{2l+4}k^3}\frac{\gamma_{\mathrm{D}}\,\omega\,\omega_{\mathrm{P}}^2\left(\omega^2-\frac{l+1}{2l+1}\omega_{\mathrm{P}}^2\right)\left(\omega^2-\frac{1}{2}\omega_{\mathrm{P}}^2\right)}{\left(\omega^2-\omega_{l+}^2\right)^2\left(\omega^2-\omega_{l-}^2\right)^2+\gamma_{\mathrm{D}}^2\omega^2\left(2\omega^2-\omega_{\mathrm{P}}^2\right)^2}(A^{2l+1}-a^{2l+1}). \quad \text{(A5)}$$

If we deconvolute each peak by expanding the term $(\omega^2-\omega_{l\pm}^2)^2$ into the form $(\omega-\omega_{l\pm})^2(\omega+\omega_{l\pm})^2$ and set $\omega=\omega_{l\pm}$ everywhere but in the factor $(\omega-\omega_{l\pm})^2$, we recover Eq. (11), with its characteristic Lorentzian-shaped character. All terms, including effective volumes, coincide exactly in the two cases.

[1] E. Purcell, Phys. Rev. **69**, 681 (1946).
[2] M. I. Stockman, Opt. Express **19**, 22029 (2011).
[3] S. Gaponenko, *Introduction to Nanophotonics* (Cambridge University Press, Cambridge, 2010).
[4] B. Huttner, J. J. Baumberg, and S. M. Barnett, Europhys. Lett. **16**, 177 (1991).
[5] H. T. Dung, L. Knöll, and D. G. Welsch, Phys. Rev. A **57**, 3931 (1998).
[6] O. Di Stefano, S. Savasta, and R. Girlanda, Phys. Rev. A **61**, 023803 (2000).
[7] H. T. Dung, L. Knöll, and D. G. Welsch, Phys. Rev. A **62**, 053804 (2000).
[8] L. Knoll, S. Scheel, and D. G. Welsch, in *Coherence and Statistics of Photons and Atoms* (Wiley, New York, 2001).
[9] J. J. Hopfield, Phys. Rev. **112**, 1555 (1958).
[10] C. Tai, *Dyadic Green Functions in Electromagnetic Theory*, 2nd ed. (IEEE Press, Piscataway, NJ, 1993).
[11] J. M. Wylie and J. E. Sipe, Phys. Rev. A **30**, 1185 (1984).
[12] N. A. R. Bhat and J. E. Sipe, Phys. Rev. A **73**, 063808 (2006).
[13] H. T. Dung, L. Knöll, and D. G. Welsch, Phys. Rev. A **64**, 013804 (2001).
[14] G. Burlak, *The Classical And Quantum Dynamics Of The Multi-spherical Nanostructures* (Imperial College Press, London, 2004).
[15] R. Carminati, J. Greffet, C. Henkel, and J. Vigoureux, Opt. Commun. **261**, 368 (2006).
[16] H. Mertens, A. F. Koenderink, and A. Polman, Phys. Rev. B **76**, 115123 (2007).
[17] L.-W. Li, M.-S. Leong, P.-S. Kooi, and T.-S. Yeo, IEEE Trans. Antennas Propag. **49**, 645 (2001).
[18] D. Guzatov and V. Klimov, Chem. Phys. Lett. **412**, 341 (2005).
[19] T. V. Teperik, V. V. Popov, and F. J. García de Abajo, Phys. Rev. B **69**, 155402 (2004).
[20] A. Moroz, Ann. Phys. **315**, 352 (2005).
[21] A. Moroz, Chem. Phys. **317**, 1 (2005).
[22] D. E. Chang, A. S. Sørensen, P. R. Hemmer, and M. D. Lukin, Phys. Rev. B **76**, 035420 (2007).
[23] R. Chance, A. Prock, and R. Silbey, Adv. Chem. Phys. **37**, 1 (1978).
[24] Y. S. Kim, P. Leung, and T. F. George, Surf. Sci. **195**, 1 (1988).
[25] R. X. Bian, R. C. Dunn, X. S. Xie, and P. T. Leung, Phys. Rev. Lett. **75**, 4772 (1995).
[26] L. Novotny, Appl. Phys. Lett. **69**, 3806 (1996).
[27] A. Rahmani, P. C. Chaumet, F. de Fornel, and C. Girard, Phys. Rev. A **56**, 3245 (1997).
[28] A. Rahmani, P. C. Chaumet, and F. de Fornel, Phys. Rev. A **63**, 023819 (2001).
[29] C. Hermann and O. Hess, J. Opt. Soc. Am. B **19**, 3013 (2002).
[30] M. Thomas, J. J. Greffet, R. Carminati, and J. R. Arias-Gonzalez, Appl. Phys. Lett. **85**, 3863 (2004).
[31] S. D'Agostino, P. P. Pompa, R. Chiuri, R. J. Phaneuf, D. G. Britti, R. Rinaldi, R. Cingolani, and F. D. Sala, Opt. Lett. **34**, 2381 (2009).
[32] A. Mohammadi, F. Kaminski, V. Sandoghdar, and M. Agio, Int. J. Nanotechnology **6**, 902 (2009).
[33] U. Hohenester and A. Trügler, Comput. Phys. Commun. **183**, 370 (2012).
[34] H. Raether, *Surface Plasmons on Smooth and Rough Surfaces and on Gratings*, Springer Tracts in Modern Physics Vol. 111 (Springer, Berlin, 1988).
[35] F. Garcia-Moliner and F. Flores, *Introduction to the Theory of Solid Surfaces* (Cambridge University Press, Cambridge, 1979).
[36] S. A. Maier, Opt. Express **14**, 1957 (2006).
[37] M. Agio, Nanoscale **4**, 692 (2012).
[38] M. Babiker and G. Barton, J. Phys. A **9**, 129 (1976).
[39] G. Barton, Rep. Prog. Phys. **42**, 963 (1979).
[40] E. Prodan and P. Nordlander, J. Chem. Phys. **120**, 5444 (2004).
[41] G. Sun and J. B. Khurgin, IEEE J. Sel. Top. Quantum Electron. **17**, 110 (2011).
[42] J. Steele, N. Grady, P. Nordlander, and N. Halas, in *Surface Plasmon Nanophotonics*, edited by M. Brongersma and P. Kik (Springer, Berlin, 2007), pp. 183–196.
[43] C. Vandenbem, D. Brayer, L. S. Froufe-Pérez, and R. Carminati, Phys. Rev. B **81**, 085444 (2010).
[44] V. Klimov and D. Guzatov, Appl. Phys. A **89**, 305 (2007).
[45] V. Klimov and A. Lambrecht, Plasmonics **4**, 31 (2009).
[46] G. Sun and J. B. Khurgin, Appl. Phys. Lett. **97**, 263110 (2010).
[47] V. Yannopapas, A. Modinos, and N. Stefanou, Phys. Rev. B **60**, 5359 (1999).
[48] A. Trügler and U. Hohenester, Phys. Rev. B **77**, 115403 (2008).
[49] E. Waks and D. Sridharan, Phys. Rev. A **82**, 043845 (2010).
[50] C. Van Vlack, P. T. Kristensen, and S. Hughes, Phys. Rev. B **85**, 075303 (2012).
[51] S. Savasta, R. Saija, A. Ridolfo, O. Di Stefano, P. Denti, and F. Borghese, ACS Nano **4**, 6369 (2010).
[52] F. H. L. Koppens, D. E. Chang, and F. J. García de Abajo, Nano Lett. **11**, 3370 (2011).
[53] L.-W. Li, P.-S. Kooi, M.-S. Leong, and T.-S. Yee, IEEE Trans. Microwave Theory Tech. **42**, 2302 (1994).
[54] E. Prodan and P. Nordlander, Chem. Phys. Lett. **352**, 140 (2002).
[55] J. Jackson, *Classical Electrodynamics*, 3rd ed. (Wiley, New York, 1999).
[56] It has been obtained by a parametric fit of the Drude dielectric function over the experimental data provided by Palik,[77] with the additional constraint $\epsilon_{\text{Drude}}(\omega_{\text{SP}}) = \epsilon_{\text{exp}}(\omega_{\text{SP}}) = -1$, intended to make the surface plasmon frequency ω_{SP} coincide exactly with the experimental value.
[57] E. Prodan, C. Radloff, N. J. Halas, and P. Nordlander, Science **302**, 419 (2003).
[58] The integral in Eq. (9) is always convergent in the case of nanoshells, because the electric field in the exterior of the shell decays as $r^{-(l+2)}$ [see Eq. (2)]. In general, we think that the convergence of the integral is guaranteed as long as a family of *localized* modes of the field exists, which holds true in the case of confined metallic nanostructures.
[59] L. D. Landau and E. M. Lifshitz, *Electrodynamics of Continuous Media*, 2nd ed. (Pergamon, Oxford, 1984).
[60] For more details about the calculations, see: F. Alpeggiani, Master's thesis, University of Pavia, 2012.
[61] G. Colas des Francs, S. Derom, R. Vincent, A. Bouhelier, and A. Dereux, Int. J. Optics **2012**, 1 (2012).
[62] A. F. Koenderink, Opt. Lett. **35**, 4208 (2010).
[63] P. Yao, C. Van Vlack, A. Reza, M. Patterson, M. M. Dignam, and S. Hughes, Phys. Rev. B **80**, 195106 (2009).
[64] P. W. Milonni and P. L. Knight, Phys. Rev. A **10**, 1096 (1974).
[65] L. C. Andreani, G. Panzarini, and J. M. Gérard, Phys. Rev. B **60**, 13276 (1999).
[66] H. J. Carmichael, R. J. Brecha, M. G. Raizen, H. J. Kimble, and P. R. Rice, Phys. Rev. A **40**, 5516 (1989).

[67]T. Ochiai, J.-I. Inoue, and K. Sakoda, Phys. Rev. A **74**, 063818 (2006).
[68]R. Ruppin, Phys. Rev. B **45**, 11209 (1992).
[69]M. Boustimi, J. Baudon, and J. Robert, Opt. Commun. **198**, 389 (2001).
[70]I. A. Larkin, M. I. Stockman, M. Achermann, and V. I. Klimov, Phys. Rev. B **69**, 121403 (2004).
[71]E. Castanié, M. Boffety, and R. Carminati, Opt. Lett. **35**, 291 (2010).
[72]J. M. McMahon, S. K. Gray, and G. C. Schatz, Nano Lett. **10**, 3473 (2010).
[73]K. Busch and S. John, Phys. Rev. Lett. **83**, 967 (1999).
[74]F. Intonti, S. Vignolini, F. Riboli, A. Vinattieri, D. S. Wiersma, M. Colocci, L. Balet, C. Monat, C. Zinoni, L. H. Li, R. Houdré, M. Francardi, A. Gerardino, A. Fiore, and M. Gurioli, Phys. Rev. B **78**, 041401 (2008).
[75]A. Weber-Bargioni, A. Schwartzberg, M. Cornaglia, A. Ismach, J. J. Urban, Y. Pang, R. Gordon, J. Bokor, M. B. Salmeron, D. F. Ogletree, P. Ashby, S. Cabrini, and P. J. Schuck, Nano Lett. **11**, 1201 (2011).
[76]W. Chen, A. Kirilyuk, A. Kimel, and T. Rasing, Appl. Phys. Lett. **100**, 163111 (2012).
[77]E. Palik, *Handbook of Optical Constants of Solids* (Academic, New York, 1985), Vol. 1.